Check for updates

ADVANCED FUNCTIONAL MATERIALS
www.afm-journal.de

Light-Controlled Reversible Coassembly of Hybrid Functional Nanostructures

Michal Sawczyk, Yanxiao Han, Soumyo Sen, Bartosz Smereczyński, Petr Král,* and Michał M. Wójcik**

Reversible coassembly of hybrid low-dimensional nanostructures offers a route to tunable materials for sensing, separation, delivery, and catalysis. However, many functional nanoscale building blocks are stabilized by aromatic ligands and suffer from poor solubility, intermolecular π stacking, and limited chemical stability. Here, a light-controlled platform is introduced that couples photoisomerizable azobenzene ligands with polycyclic aromatic hydrocarbon (PAH)-functionalized counterparts to switch the interparticle coupling in heterogeneous mixtures. The strategy uses complementary electron-rich and electron-deficient sites generated on different nanocomponents, providing mild charge-transfer interactions that drive reversible coassembly, while maintaining the balance between attractive and repulsive forces. Using this mechanism, nanocomposites are prepared including gold NPs with magnetite (Fe_3O_4) NPs and gold NPs with carbon nanotubes. An external magnetic field can further direct Fe_3O_4-containing hybrids and enables noninvasive separation. This system requires no chemical additives, and produces on-demand transitions with photo-modulated optical and magnetic responses, advancing stimuli-responsive assembly beyond conventional electrostatic, thermal, solvent, or redox controls.

1. Introduction

Reversible coassembly of mixed low-dimensional (low-D) colloidal building blocks—defined as nanoscale objects with at least one confined dimension, including 0D nanoparticles (NPs),[1–4] 1D nanotubes (NTs) or nanorods,[5] and 2D nanosheets—allows the preparation of functional materials with switchable structures and properties. Such multiscale hybrids can form nanocrystalline lattices, hydrogels,[6] porous networks,[7,8] and other composites[9] with tunable optical, electronic, mechanical, and magnetic characteristics.[10–14] Their dynamic assembly states give rise to applications in molecular sensing, supramolecular separations,[4,15] storage and controlled release,[16,17] and catalysis.[18–20] In addition, the formulation of these nanocomposites can be tuned to merge the unique properties of different building blocks, enabling selective coassembly with both molecular species and other low-D components. This enables capture and on-demand release of chemical reactants and NPs, including catalyst carriers, drug-delivery vesicles, sorbents for targeted removal, and composites integrating well-defined functions of specific nanostructures.

Despite these advantages, reversible coassembly of dissimilar nanostructures with tunable composition and morphology remains challenging. A general strategy is to modulate, in situ, the solvation and interparticle interactions imparted by surface-anchored ligands.[23] Interacting ligands, whether identical or complementary, must provide chemically stable interfaces with binding energies sufficient to compete with solvation, which makes their design nontrivial. Electrostatic interactions, switchable ligand polarity, and hydrogen-bonded pairing, including polymer- and DNA-inspired motifs, are among the most established solutions (**Table 1**). However, the reactivity of these ligands often complicates repeated cycling and chemical compatibility, for instance, with catalysts. Ideally, cointeracting ligands would form complementary pairs whose mutual affinity can be toggled by a controllable conformational change. A promising direction is the use of less reactive, purely noncovalent pairs that assemble via mild charge-transfer interactions, creating electron-rich and electron-deficient sites on different nanoscale components that

M. Sawczyk, B. Smereczyński, M. M. Wójcik
Faculty of Chemistry
University of Warsaw
Pasteura 1, Warsaw 02-093, Poland
E-mail: msawczyk@umich.edu; mwojcik@chem.uw.edu.pl

M. Sawczyk, Y. Han, S. Sen, P. Král
Department of Chemistry
University of Illinois at Chicago
Chicago, IL 60607, USA
E-mail: pkral@uic.edu

P. Král
Department of Physics
Pharmaceutical Sciences, and Chemical Engineering
University of Illinois at Chicago
Chicago, IL 60607, USA

The ORCID identification number(s) for the author(s) of this article can be found under https://doi.org/10.1002/adfm.202504830

© 2025 The Author(s). Advanced Functional Materials published by Wiley-VCH GmbH. This is an open access article under the terms of the Creative Commons Attribution License, which permits use, distribution and reproduction in any medium, provided the original work is properly cited.

DOI: 10.1002/adfm.202504830

Table 1. Reversible coassembly strategies in hybrid nanosystems driven by different stimuli.

System (nanocarriers + ligands)	Dominant intercomponent interactions	Primary trigger(s)	Reversibility/selectivity notes	Refs.
Au NPs (azo ligands) + Fe_3O_4 NPs (catechol-PAH ligands); CNTs (PAH ligands)	π stacking (pyrene > naphthalene > benzene); (*Z*)-azo lone-pair–π; vdW	Light (*E*↔*Z* isomerization); magnetic field (superferromagnetism)	Reversible; aromaticity dictates selectivity; selective NPs decoration on CNT walls; solvent-sensitive	This work
Au NPs (azo, spiropyran, photoacid ligands; NPs same or complementary); SiO_2 NPs; Fe_3O_4 NPs	Ligand polarity; solvophobic shift; π stacking; reversible protonation; short-range electrostatics	Light (molecular photoswitching); magnetic field (superferromagnetism)	Reversible in most cases; Irreversible for DASA; high reactivity of spiropyrans; solvent-sensitive	[4,22,31,44,53]
Azobenzene + graphene composites; NPs + graphenes; Au NPs + Fe_3O_4 NPs	Ligand polarity; vdW attraction; hydrogen bonding	Light (*E*↔*Z* isomerization); redox (in situ deposition)	Irreversible or reversible; trapping of polar NPs; light controls graphene exfoliation and binding; strong vdW stacking	[55,56,62,64]
Mixed NPs; graphene-coated NPs + pyrene-NHC; Au NPs + liquid crystals/polymers	π stacking; vdW; hydrogen bonding	Temperature (phase transition, breaking supramolecular bonds); light (molecular photoswitching)	Reversible; trapping and release of catalysts; LC-controlled NPs self-organization	[21,54,58,60,61]
Metallic NPs + CNTs; CNTs-organic hybrids; Fe_3O_4-CNTs composites	vdW forces; π stacking	None (spontaneous); redox (in situ deposition); magnetic field	Irreversible	[63,66,67]
Mixed NPs 2D lattices; 3D superstructures; Au NPs + DNA composites; organic–inorganic supraparticles	Electrostatic forces; vdW; hydrogen bonding	Ionic strength; pH; temperature	Irreversible (in most cases)	[57,59,65,68]

reversibly attract each other while balancing attractive and repulsive forces.

The ligands capable of sufficiently strong noncovalent cobinding can rely on polycyclic aromatic hydrocarbons (PAHs) and their derivatives, however, inherent π stacking hampers their solubility and hinders controllable assembly, even in aromatic solvents.[24–27] Such ligands are generally chemically stable unless they comprise reactive organic groups; certain PAHs, such as extended acenes, are prone to oxidation and side reactions,[24,25] these stability issues can limit their broad-range deployment. Prior stimuli such as temperature,[21] solvent polarity,[28] ionic strength, and redox bias[29,30] can trigger assembly–disassembly cycles but often at the cost of chemical additives, poor selectivity, or compatibility issues. In contrast, light-controlled modulation of weak noncovalent interactions offers spatial and temporal precision with minimal medium perturbation,[22,23] while avoiding reactive functional groups, such as amines, imines, carboxylic acids, phenols, or chinones, that may induce irreversible side reactions compromising ligand functionality and system stability.

Here, we introduce a light-controlled self-assembly platform in which photoisomerizable azobenzene ligands are combined with nonreactive PAH-functionalized components to toggle solubility and interparticle coupling within binary mixtures. Using this strategy, we reversibly coassemble multicomponent mixtures of low-D nanostructures: gold NPs with magnetite (Fe_3O_4) NPs and gold NPs with carbon nanotubes (CNTs), wherein one nanocomponent bears azobenzene ligands and the other distinct aromatic ligands. An external magnetic field provides an orthogonal handle to direct Fe_3O_4-containing assemblies and perform magnetic separation of the resulting materials. The on-demand transitions between dispersed and coassembled states enable photomodulated optical and magnetic responses and a non-invasive separation strategy, features directly relevant to the application areas above.[4,15–20]

This work advances stimuli-responsive coassembly by: i) enabling reversible, aromaticity-controlled coassembly across dissimilar low-D building blocks, ii) employing an optical stimulus to modulate solvation and interparticle coupling without chemical additives or reactive ligands, and iii) introducing orthogonal magnetic control for directional assembly and post-assembly separation. For context, we provide a concise comparison to thermal-, solvent-, and redox-controlled strategies (Table 1), highlighting selectivity in mixed systems, compatibility with PAH ligands, and common limitations.[21–30]

2. Mutual Coupling of Photoactive Ligands

Recently, gold NPs functionalized with azobenzene and spiropyrans of phototunable polarity have been used as a convenient model for reversible self-assembly in organic media, such as toluene and methanol.[4,31] As an example, NPs decorated with essentially nonpolar (*E*)-azobenzene ligands tend to be well solvated in toluene. Once the ligands are switched by ≈365 nm ultraviolet light to the more polar *(Z)*-azobenzene form, the ligands gain significant dipolar moment. The photoinduced change of the ligand polarity significantly hampers the solvation of these NPs due to the spatial inability to accommodate solvating toluene molecules. As a result, the functionalized NPs rapidly self-assemble into spheroidal aggregates, while simultaneously being able to trap other polar guest molecules dissolved in the system. An inverse tendency can be observed in highly polar protic solvents, such as water.[32] For instance, NPs decorated with highly polar

© 2025 The Author(s). Advanced Functional Materials published by Wiley-VCH GmbH

16163028, 0, Downloaded from https://advanced.onlinelibrary.wiley.com/doi/10.1002/adfm.202504830 by Readcube (Labtiva Inc.), Wiley Online Library on [10/1/2025]. See the Terms and Conditions (https://onlinelibrary.wiley.com/terms-and-conditions) on Wiley Online Library for rules of use; OA articles are governed by the applicable Creative Commons License

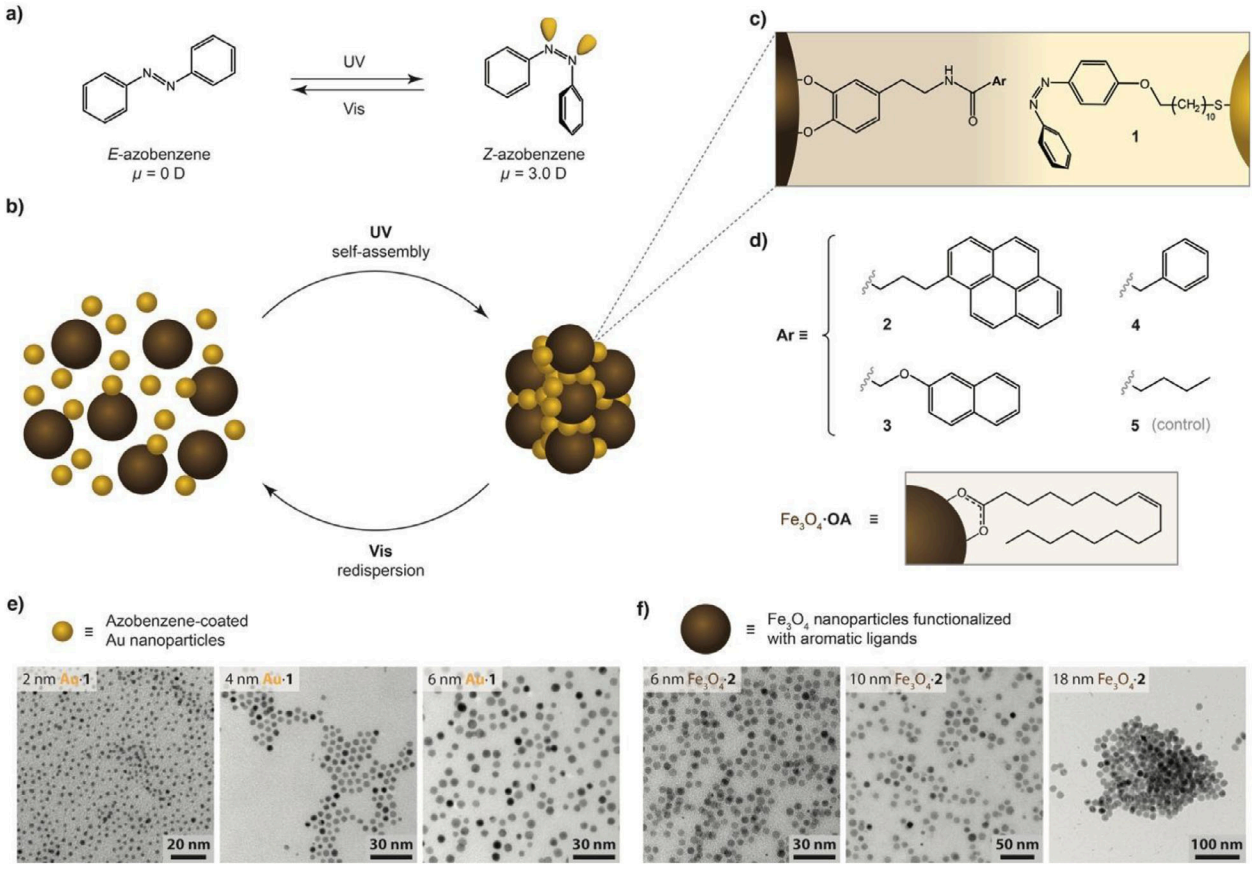


Figure 1. Light-driven coassembly of "aromatic" magnetite NPs and photoresponsive Au NPs in toluene. a) Azobenzene isomerization is accompanied by a change of molecular dipole moment. b) Schematic representation of NPs coassembly and c) interparticle binding motif. d) Chemical formulas of ligands immobilized on Fe_3O_4 NPs surface. TEM images of e) Au NPs and f) Fe_3O_4 NPs employed in self-assembly.

merocyanine (MC) ligands remain well solvated in aqueous environments, while rapidly aggregating upon light-induced MC photoisomerization to essentially nonpolar spiropyran. However, it is unclear if NPs covered with such photoactive ligands could coassemble with other nanostructures functionalized with intrinsically different aromatic ligands, based on mild noncovalent interactions between nanoscale building blocks, contributing to their controllable coassembly into larger superstructures.

Besides well-studied π-stacking, other supramolecular interactions could contribute to the cobinding of aromatic molecules, such as an electron transfer between lone pairs of (*Z*)-azobenzene and electron-deficient centers within extended aromatic rings. The lone pair–π and anion–π (or, in general, dipole–π) interactions were reported in numerous supramolecular complexes.[33,34] However, such a lone pair-π attraction has not been directly harnessed to prepare supramolecular nanostructures, despite the evidence of a significant role played by a lone pair-π stabilizing coordination complexes and various macromolecules, like *Z*-DNA and proteins.[35,36] This can be rationalized by the general weakness of such bonding, typically being overcome by much stronger solvation effects. Nevertheless, the lone pair–π interaction has been shown to drive the reactivity of small molecules[37,38] and their reversible trapping under nanoconfinement,[4] further encouraging more detailed studies.

We anticipated that NPs with surface-immobilized (*Z*)-azobenzene, comprising two neighboring lone pairs on nitrogen atoms, could interact with other nanostructure-supported polycyclic aromatic units, thus providing the attractive force for their coassembly. Hence, we conceived the idea of a system composed of magnetite NPs functionalized with polycyclic aromatic ligands and photoswitchable azobenzene-coated Au NPs, which upon ultraviolet irradiation could reversibly coassemble into metastable superstructures. This coassembly could be enabled by the initial (*E*)-to-(*Z*) isomerization of azobenzene and subsequent azobenzene polarity change,[4,23] followed by their attraction to polycyclic aromatic ligands, inducing the coassembly of both types of NPs and expelling solvent molecules from the confined spaces between both NPs. The photoswitched ligands attached to the Au and Fe_3O_4 NPs surfaces would interact by multivalent π–π and lone pair-π interactions, as shown in **Figure 1**a–d.

3. Light-Induced Coassembly of Aromatic Nanoparticles

To test these ideas, we first synthesized gold NPs of three distinct sizes (2 nm, 4 nm, and 6 nm Au·1) functionalized with azobenzene (Figure 1e; Figure S7, Supporting Information). Upon

© 2025 The Author(s). Advanced Functional Materials published by Wiley-VCH GmbH

16163028, 0, Downloaded from https://advanced.onlinelibrary.wiley.com/doi/10.1002/adfm.202504830 by Readcube (Labtiva Inc.), Wiley Online Library on [10/11/2025]. See the Terms and Conditions (https://onlinelibrary.wiley.com/terms-and-conditions) on Wiley Online Library for rules of use; OA articles are governed by the applicable Creative Commons License

exposure to UV irradiation in nonpolar solvents, such as toluene,[39] these NPs exhibited reversible self-assembly, forming spherical aggregates ranging from 200–400 nm in diameter (see Figures S37 and S38, Supporting Information). Next, we synthesized magnetite NPs[40] of three sizes (6, 10 and 18 nm Fe_3O_4, Figure 1f) decorated with aromatic ligands **2–4** comprising pyrene, naphthalene, and benzene units, where the catechol moiety was used as an anchor covalently binding to the magnetite surface.[41] Anthracene was excluded from this library due to rapid dimerization upon UV irradiation,[42] particularly facilitated when immobilized on NPs surfaces.[43] At these sizes, magnetite NPs should be superparamagnetic at room temperature (magnetic anisotropy barriers are smaller than the thermal k_BT energy). The magnetic dipole–dipole coupling energy (E_d) between two NPs is quadratically dependent on the particle dipole moment,[44,45]

$$E_d \approx \frac{\mu_0 \mu^2}{4\pi d^3} \quad (1)$$

where μ is magnetic dipole moment (proportional to NP volume), d is the average distance between two particles, and μ_0 is the permeability of free space. To keep such NPs freely soluble, E_d should be smaller than the thermal energy k_BT, which is typically an order of magnitude larger than E_d in NPs smaller than ≈25 nm at room temperature.[45,46] Since the magnetic dipole-dipole coupling alone is not sufficient for the aggregation of smaller magnetite NPs, small 6 nm and 10 nm Fe_3O_4 NPs covered by aromatic ligands **2–4**, formed stable dispersions in toluene and did not react to a permanent neodymium magnet in dark, ultraviolet or visible light. In contrast, 18 nm magnetite NPs remained assembled into ≈200 nm clusters due to extensive magnetic dipolar coupling and stronger interparticle π stacking between many aromatic ligands. Such clusters of 18 nm NPs assemblies could be magnetically separated from the dispersion due to oriented frozen superspins of the whole aggregates. The stability of 6–10 nm Fe_3O_4 NPs dispersions could be explained by relatively large surface area occupied by a single ligand on the NPs with sufficiently high curvature (Table S1, Supporting Information; 0.495–0.590 nm^2 for 6–10 nm NPs). Compared to aliphatic ligands with one-atom binding site (0.16 to 0.23 nm^2),[52] this extra space between the ligands allowed toluene molecules to sufficiently solvate the aromatic ligands to make the 6-10 nm NPs well-soluble. Catechol unit used as anchor binding to Fe_3O_4 surface covalently binds to iron atoms making the ligand attachment chemically stable.[40,41,44] Lower NPs curvature in 18 nm NPs expectedly resulted in higher ligand grafting density (0.34–0.42 nm^2) and their insolubility in any common organic solvent.

It was unknown whether the azobenzene-functionalized Au·**1** NPs and any of the 6 nm or 10 nm Fe_3O_4 NPs would coassemble into binary conglomerates upon UV irradiation. One could expect that Au NPs would self-assemble in the same manner as they had been irradiated alone. However, if the aromatic ligands **2–4** on Fe_3O_4 NPs had sufficiently large mutual binding energy to the photoisomerized *(Z)*-azobenzene moieties on Au NPs, then these NPs would form metastable nanocomposites with specific Au-to-Fe_3O_4 ratios. The experiments have shown that when a mixture of pyrene-coated 6 nm magnetite NPs (Fe_3O_4·**2**) and 4 nm Au·**1** NPs was exposed to a low intensity (≈3.5 mW cm^{-2}) ultraviolet lamp, these NPs indeed coassembled and formed ferromagnetic aggregates (**Figure 2**a,c). The growth of sub-micrometer assemblies was accompanied by the increased absorption above ~600 nm due to the Rayleigh and Mie scattering effects.[47] The bathochromic shift of the localized surface plasmon resonance (LSPR) peak from 525 to ~560 nm is typical for the formation of spherical Au NP assemblies.[48] The aggregates could be easily separated from the solution using a permanent neodymium magnet (Figure 2a,b,d) due to the interlocked magnetic spin within such Au- Fe_3O_4 clusters, where Au NPs worked as a "glue" between the trapped Fe_3O_4 NPs. The process was fully reversible: when exposed to visible light, all NPs redispersed even in the presence of magnetic field (Figure S41, Supporting Information). The cycle could be repeated at least 8 times without any trace of fatigue (Figure 2b; Figure S41, Supporting Information). Similar results were obtained upon analogous irradiation of a system composed of 6 nm and 10 nm Fe_3O_4 NPs functionalized with ligands **3** or **4**, and 4 nm Au·**1** NPs. Transmission (TEM) and scanning (SEM) electron microscopy images (Figure 2c; Figure S42, Supporting Information) indicated that the typical size of assemblies ranged between 90 and 200 nm. Their finite spherical morphology suggested that the surface electrostatics could be a self-limiting growth factor, as essentially polar (*Z*)-azobenzene layer on the NPs surface can prevent from an infinite superstructure elongation. However, we noticed that the extended irradiation times (≈15 min) and hampering the NP solvation effects by adding hexane would result in the formation of larger, branched aggregates (Figure S49, Supporting Information).

We quantified the composition of aggregates comprising trapped "aromatic" magnetite NPs ($\chi = n_{Au\ NPs}/n_{Fe3O4\ NPs}$) by irradiating equimolar Au/Fe_3O_4 NPs mixtures and collecting the self-assembled structures by centrifugation. The excess of superparamagnetic iron oxide NPs remained in the supernatants. After washing the assemblies with toluene in dark and decomposing the NPs in diluted aqua regia, we analyzed the Au and Fe content using inductively coupled plasma mass spectrometry (ICP-MS) and colorimetry based on the UV/Vis absorbance intensity (Section S11, Supporting Information). We found the gold-to-magnetite ratio varying between $4.4 < \chi < 218$, depending on the NPs dimensions and aromatic ligand used. In all cases the trend clearly indicated exponentially decreasing magnetite content when the aromatic ring size decreased from pyrene, naphthalene, and benzene, respectively (Table S1, Supporting Information). The average values were $\chi = 6.6 \times 10^0$, 3.9×10^1, and 1.5×10^2 for NPs systems comprising ligands **2**, **3** and **4**, respectively. Therefore, we assumed that the extension of aromatic ring from benzene towards pyrene assured significantly stronger attraction between polar (*Z*)-**1** ligand and aromatic groups of progressively increasing π conjugation (Figure 2d,e).

4. Modeling of Coupling between Aromatic Ligands

To better understand the molecular interactions between azobenzene isomers and PAHs used in the experiments, we carried out ab initio calculations of the conformations and coupling energies of these moieties. **Figure 3** reveals the conformations of the coupled aromatic molecules and **Table 2** shows their

© 2025 The Author(s). Advanced Functional Materials published by Wiley-VCH GmbH

16163028, 0, Downloaded from https://advanced.onlinelibrary.wiley.com/doi/10.1002/adfm.202504830 by Readcube (Labtiva Inc.), Wiley Online Library on [10/11/2025]. See the Terms and Conditions (https://onlinelibrary.wiley.com/terms-and-conditions) on Wiley Online Library for rules of use; OA articles are governed by the applicable Creative Commons License

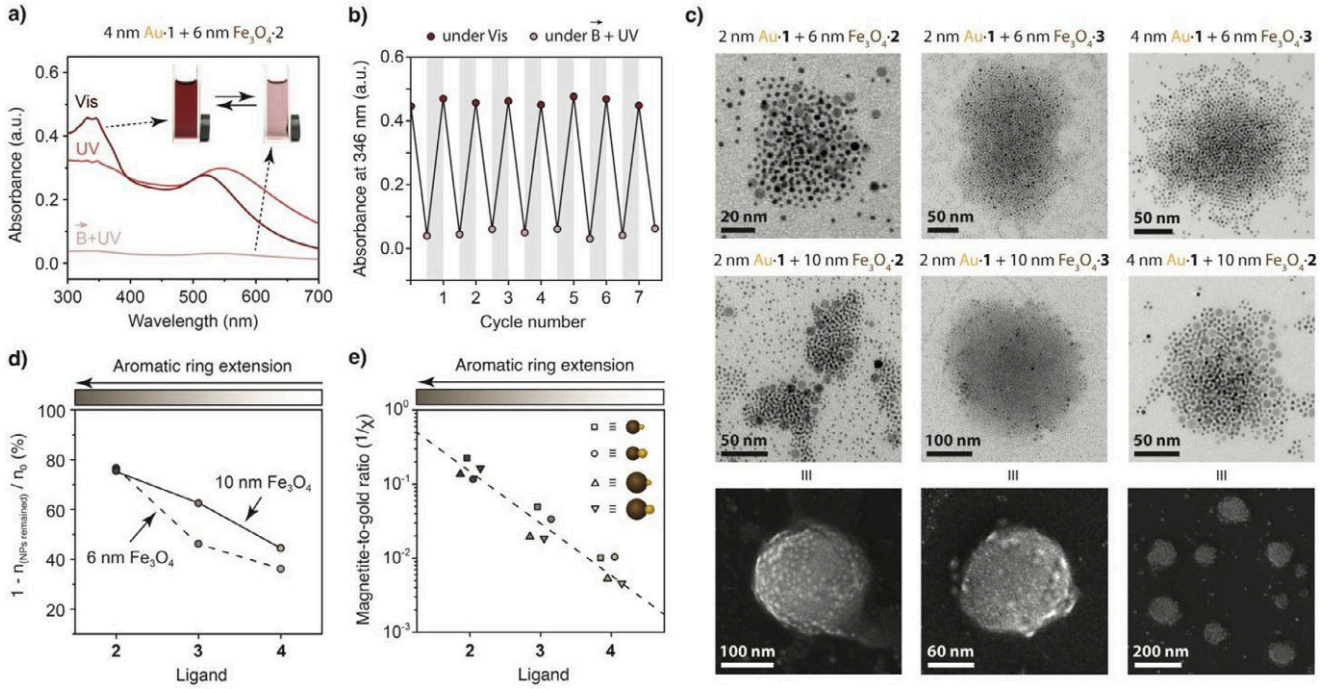


Figure 2. Reversibility and properties of the Au/Fe_3O_4 assemblies. a) UV/Vis absorption spectra accompanying the UV light-induced self-assembly and subsequent magnetic separation of the aggregates. The inset pictures show the red NPs dispersion under visible light (left) and assemblies separated by a magnet under UV light (right). b) Reversibility of the coassembly process monitored by UV/Vis. c) Top, TEM; and bottom, SEM images of different Au/Fe_3O_4 coassemblies after UV illumination show the trapping of magnetite NPs within aggregated Au NPs. d) Percentage of NPs removed from the solutions after magnetic separation carried out under UV light. e) Composition of Au/Fe_3O_4 assemblies represented as $N_{Fe3O4\ NPs}/N_{Au\ NPs}$ ratio.

interaction energies. Interestingly, the coupling energies between (*Z*)-azobenzene and pyrene, naphthalene, and benzene are lower compared to (*E*)-azobenzene coupled with the same aromatics, indicating a lower stability of the latter. The lone pairs adjacent to nitrogen atoms in (*Z*)-azobenzene are oriented towards the electron-deficient ring centers (Figure S57, Supporting Information) within the heterodimers comprising naphthalene and pyrene, while the benzene's case was less clear. The obtained conformations and binding energies reveal significantly stronger coupling for Au·**1** Fe_3O_4 NPs modified by **2** and **3**, compared to ligand **4**. This translates into an increasing magnetite content along with the ring extension from benzene to pyrene (Figure 2e), leading to more efficient NPs magnetic separation (Figure 2d). By splitting the interaction energies into π–π and dipole–π, the latter turned out to be significantly lower in the (*E*)- than (*Z*)-enantiomers, while π–π binding energies were comparable in benzene and pyrene, and they varied in naphthalene.

5. Aromaticity Influence on NPs Coassembly

We conducted the additional experiments to assess the binding capacity of "non-aromatic" NPs, specifically those functionalized with short aliphatic chains (Fe_3O_4·**5**), and pristine oleic acid-stabilized magnetite NPs (Fe_3O_4·OA), with the self-assembling Au·**1** NPs. Unfortunately, Fe_3O_4·**5** dispersions in either toluene or toluene/hexane mixtures were rather unstable and spontaneously aggregated in this environment due to hampered solvation of the short ligand; this excluded Fe_3O_4·**5** NPs from reproducible experiments. Therefore, we used stable and well-soluble Fe_3O_4·OA NPs as a control system. As expected, such NPs did not coassemble in the presence of Au·**1** NPs when exposed to UV light (Figure S53, Supporting Information) and the produced Au NP-aggregates could not be magnetically separated. Hence, the coupling between azobenzene ligands and aliphatic chains in OA were relatively weak, in contrast to the aromatic ligands **2**–**4**.

Although pure Au NPs assemblies could not be magnetically separated from dispersions, here, the magnetite NPs content in the self-assembled structures as low as ≈1% allowed for their partial magnetic separation from the solution (Figure 2d; Figures S39 and S40, Supporting Information). This could be explained by the weakly paramagnetic character of gold NPs,[49,50] which, besides their role as a "glue" merging Fe_3O_4 NPs, could increase the overall magnetization of the assemblies comprising certain amount of Fe_3O_4. Moreover, it was possible to perform magnetically driven NPs self-assembly to obtain nanowire-like nanostructures primarily composed of Au NPs of 150–450 nm in diameter and 0.5–2 µm in length (**Figure** 4c,d,g; Figure S44, Supporting Information). However, elongated superstructures were not observed when magnetite NPs decorated with ligands **3** and **4** were employed, possibly due to insufficient magnetite content, i.e., ≈2.5% versus ≈16% for **2** and **3**, respectively. The absence of significant magnetite contribution in pure Au NPs assemblies resulted in their unresponsiveness to a permanent magnetic field. Consequently, it could be inferred that the paramagnetic properties of Au NPs alone are insufficient to produce assemblies with a magnetization level high enough to influence their morphology using relatively weak magnetic fields.

© 2025 The Author(s). Advanced Functional Materials published by Wiley-VCH GmbH

16163028, 0, Downloaded from https://advanced.onlinelibrary.wiley.com/doi/10.1002/adfm.202504830 by Readcube (Labtiva Inc.), Wiley Online Library on [10/11/2025]. See the Terms and Conditions (https://onlinelibrary.wiley.com/terms-and-conditions) on Wiley Online Library for rules of use; OA articles are governed by the applicable Creative Commons License

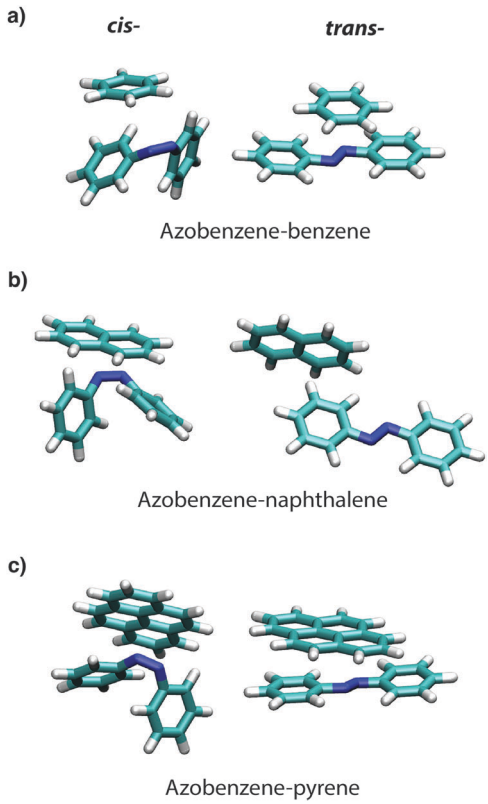


Figure 3. Ab initio optimized structures of *E*-/*Z*-azobenzene + aromatics heterodimers; a) with benzene, b) naphthalene, and c) pyrene. Extended aromatic networks in naphthalene and pyrene emphasize the possible dipole–π coupling between nitrogen's lone pairs and electron-deficient centers of polycyclic rings.

6. Magnetite Content in Self-Assembled Clusters

To demonstrate the dependence of the trapping ability on the NP-confinement, we examined the role of different sizes of Au/Fe_3O_4 NPs on the χ values. Due to the larger differences in NPs diameter, in most cases, 2 nm Au NPs could trap more Fe_3O_4. As an example, χ = 4.4, 21.0, and 99.4 for 2 nm Au + 6 nm Fe_3O_4 system, versus χ = 8.6, 28.8 and 96.4 for 4 nm Au + 6 nm Fe_3O_4 NPs modified by **2**, **3** and **4**, respectively (Figure 2e). The distribution of gold and iron in the assemblies was verified using high-angle annular dark-field scanning transmission electron microscopy (HAADF-STEM) imaging due to the electronic contrast differences between gold and magnetite (Figure 4e), as well as energy dispersive spectroscopy (EDS) mapping (Figure 4f,g). In the case of ligand **4**, the results were comparable, indicating rather a stochastic trapping of small amounts of magnetite NPs by a large excess of Au NPs. The importance of the assembly confinement can be exemplified in the behavior of 6 nm Fe_3O_4·**4**, in which only a single aromatic ring resulted in π interaction much weaker than in **2** or **3**. While 2 nm Au NPs still coassembled with 6 nm Fe_3O_4·**4** to produce magnetic aggregates (Figure S39c, Supporting Information), 6 nm Au NPs did not yield any magnetic assemblies with Fe_3O_4·**4** of the same size, and formed separate Au "islands" from which magnetite might be removed by washing (Figure S45, Supporting Information). The phenomenon can be elucidated through two main factors: i) a greater disparity in the curvature of NPs leads to more effective interlocking between the surfaces of (*Z*)-azobenzene and aromatic rings; ii) smaller gold NPs are better suited to occupy the gaps between enclosed Fe_3O_4 NPs, a configuration that is entropically favored over the entrapment of solvent molecules.

Implementing analogous self-assembly strategy for 18 nm magnetite NPs modified by **2**, **3** and **4**, we found them insoluble in any common solvent, and, therefore, they formed metastable suspensions from which they could have been easily collected with the aid of a permanent magnet. The addition of Au·**1** did not interfere with Fe_3O_4 aggregates; hence 18 nm Fe_3O_4 NPs could still be magnetically separated, while well-solvate Au NPs entirely remained dispersed in toluene. However, under UV light irradiation, we observed rapid Au NPs trapping within confined spaces of magnetite (Figures S51 and S52, Supporting Information). The morphology of these assemblies was rather inhomogeneous due to the kinetically unfavorable penetration of already aggregated magnetite NPs by Au NPs, simultaneously to the competitive agglomeration of Au NPs into distinct phases (Figure 4a,b).

Table 2. Interaction energies (in kcal/mol) between *Z*-/*E*-azobenzene isomers and differently conjugated aromatic rings: benzene, naphthalene, and pyrene.

Heterodimer	E(interaction)	*E*(lone pair-π)	*E*(π–π)
(*Z*)-azobenzene + benzene	−3.683	−1.394	−2.289
(*E*)-azobenzene + benzene	−3.387	−0.848	−2.539
(*Z*)-azobenzene + naphthalene	−6.105	−1.959	−4.146
(*E*)-azobenzene + naphthalene	−2.998	−0.471	−2.527
(*Z*)-azobenzene + pyrene	−8.689	−2.020	−6.669
(*E*)-azobenzene + pyrene	−6.520	−0.471	−6.049

7. Coassembly of Au NPs with Carbon Nanotubes

To exclude the influence of the magnetic character of iron oxide on the self-assembly, and to verify the role of the support curvature on interparticle interactions, we conceived the idea of reversible self-assembly of Au NPs onto double- and multi-walled CNTs. However, π stacking and van der Waals forces between NPs ligands and "naked" CNTs caused spontaneous, irreversible NPs adsorption on the CNTs surface. Moreover, the process was not significantly dependent on the CNTs thickness (we have tested CNTs of the diameter ranging from 2 to 20 nm), NPs diameter (from 2 to 10 nm), nor even the NPs surface functionalization (**Figure 5a**,b). Hence, we covalently functionalized multi-walled CNTs (~12 nm diameter) using diazonium chemistry[21] to yield CNTs modified with pyrene units (Figure 5c and Section S14, Supporting Information). This strategy assured a better CNTs dispersibility in organic solvents (e.g., *N*-methylpyrrolidone-toluene mixtures). Most importantly, the dispersions of modified CNTs in toluene did not adsorb Au·**1** NPs neither under visible light nor in dark. In contrast, the illumination of the samples with UV light allowed to selectively deposit the NPs on the CNTs walls, without the competitive formation of separate NPs aggregates (Figure 5d,e). Some nanotube fragments stacked to Au·**1** NPs strongly enough to produce ≈300 nm

© 2025 The Author(s). Advanced Functional Materials published by Wiley-VCH GmbH

16163028, 0, Downloaded from https://advanced.onlinelibrary.wiley.com/doi/10.1002/adfm.202504830 by Readcube (Labtiva Inc.), Wiley Online Library on [10/11/2025]. See the Terms and Conditions (https://onlinelibrary.wiley.com/terms-and-conditions) on Wiley Online Library for rules of use; OA articles are governed by the applicable Creative Commons License

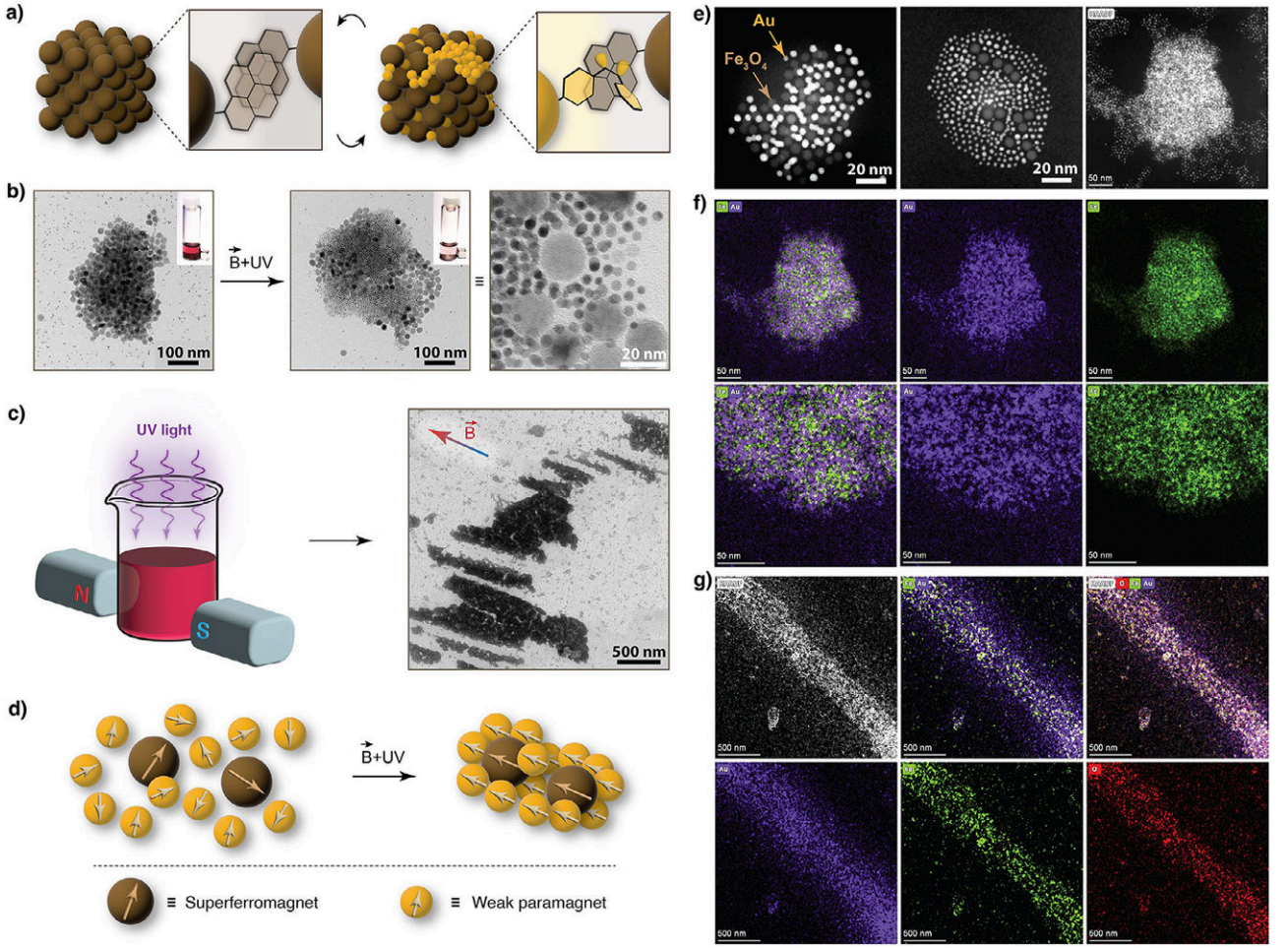


Figure 4. Influence of external magnetic field on the Au/Fe_3O_4 coassembly. a) Schematic representation of light-controlled intercalation of Au NPs within ferromagnetic 18 nm Fe_3O_4 aggregates. b) TEM images of heterogeneous 4 nm Au·**1**/18 nm Fe_3O_4·**3** mixture before (left) and after (right) UV irradiation. c,d) Simplified models and TEM image of linear assemblies obtained by UV illumination of 4 nm Au·**1**/6 nm Fe_3O_4·**2** mixture under external magnetic field applied. e) HAADF-STEM images of the coassemblies at the initial stages of photoinduced aggregation of 2 nm and 4 nm Au·**1**/6 nm Fe_3O_4·**2**. f,g) EDS maps at different magnifications showing the elemental distribution within f) spherical, and g) linear coassemblies of 4 nm Au·**1** and 6 nm Fe_3O_4·**2**.

densely packed NPs/CNTs agglomerates. Finally, the addition of a highly polar solvent, *N*-methylpyrrolidone (NMP) resulted in no self-assembly of Au NPs on the CNTs surface regardless of the UV light irradiation applied (Figure S64, Supporting Information). This indicates the strong solvation of polar (*Z*)-azobenzene units, which was much more competitive to the lone pair–π attraction between the surfaces.

We further tested whether fullerenes could interact with Au·**1** NPs under UV light. Although seemingly similar in chemical structure, fullerenes are essentially non-aromatic, unlike graphene and CNTs.[51] We thus UV-irradiated the mixtures of 6 nm Au·**1** NPs with C_{60} and C_{70} fullerenes in toluene, followed by centrifugation of as-obtained aggregates. After comparing the UV/Vis absorption spectra of supernatants with C_{60} and C_{70} solutions of concentration identical to the initial ones (Figure S58, Supporting Information), we did not observe the trapping of any amounts of both fullerenes. Due to a possible nanoconfinement mismatch, which would prevent fullerene occlusion if the NPs size was either too small or too large compared to the effective vdW diameter (e.g., ≈1.1 nm for C_{60}), we carried out analogous experiments with 2, 4, 6, 9, and 11 nm Au NPs and analyzed the supernatants by high-performance liquid chromatography (HPLC). However, in the supernatants, the amounts of both C_{60} and C_{70} were nearly identical to the initial ones before trapping, regardless of the Au NPs diameter (Figure S59, Supporting Information).

The ab initio molecular dynamics (AIMD) and computed binding energies of *(Z)*- and *(E)*-azobenzene with C_{60} at the local energy minima for different conformations (Figure S60, Supporting Information) helped to explain the experimental lack of fullerene trapping by the self-assembling Au NPs. The heterodimer orientations at the lowest energies were –1.9 and –1.2 kcal mol^{-1} for *(Z)*- and *(E)*-azobenzene, respectively (–1.65 kcal mol^{-1} vs –0.75 kcal mol^{-1} of Coulombic contribution, and –0.25 vs –0.45 kcal mol^{-1} of vdW attraction, respectively). Therefore, such small conformer difference ($\Delta E_{(E-Z)} = \approx 0.7$ kcal mol^{-1}) could easily be compensated by the solvation effects and, in fact, was significantly smaller than the corresponding energies

© 2025 The Author(s). Advanced Functional Materials published by Wiley-VCH GmbH

16163028, 0, Downloaded from https://advanced.onlinelibrary.wiley.com/doi/10.1002/adfm.202504830 by Readcube (Labtiva Inc.), Wiley Online Library on [10/11/2025]. See the Terms and Conditions (https://onlinelibrary.wiley.com/terms-and-conditions) on Wiley Online Library for rules of use; OA articles are governed by the applicable Creative Commons License

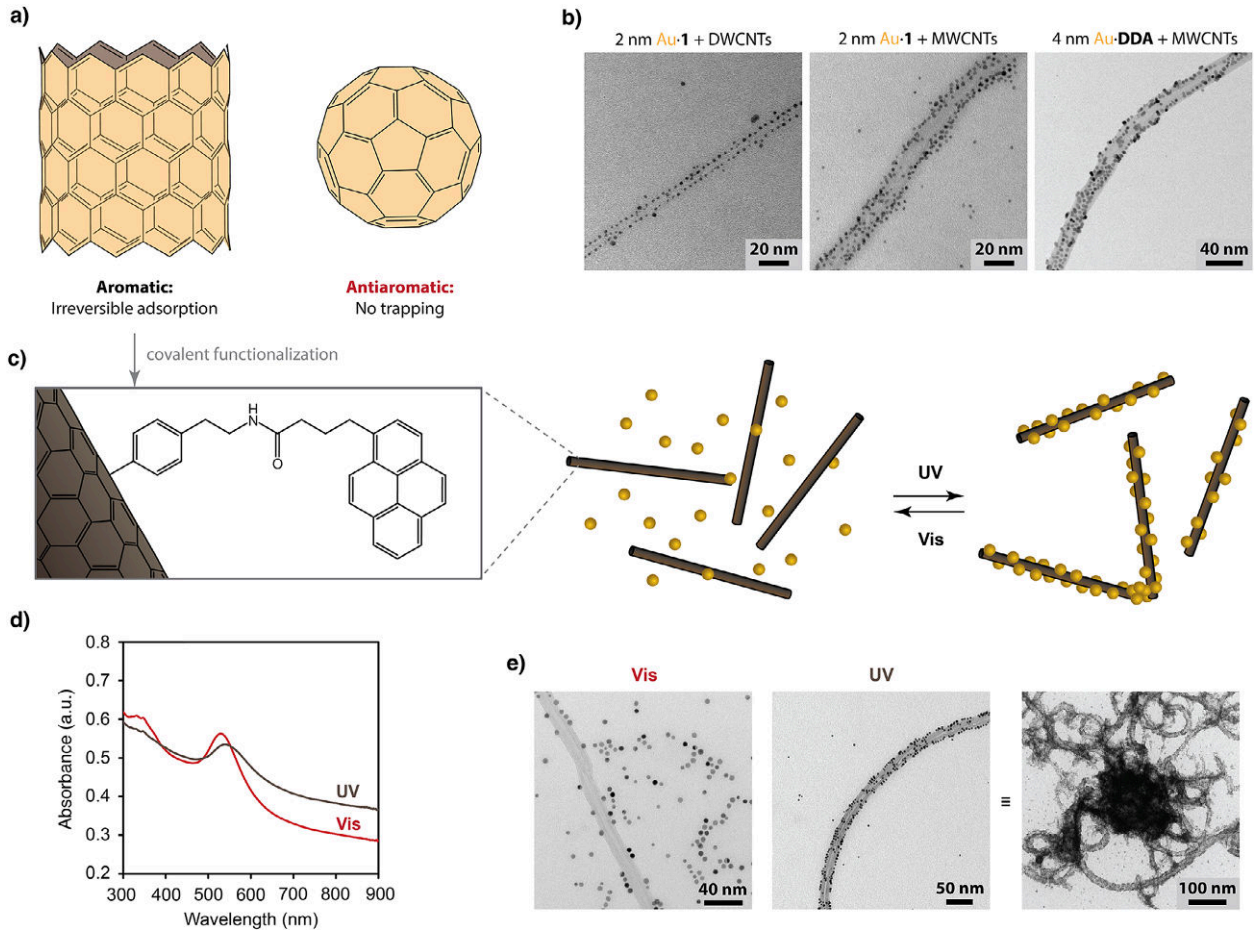


Figure 5. Coassembly of Au NPs with substrates of varying aromaticity. a,c) Simplified models of carbon nanotubes before and after functionalization. b) TEM images of 2 and 4 nm Au NPs irreversibly self-assembled (under visible light) on multiwalled CNTs and double-walled CNTs. d) UV/Vis absorption spectra and e) TEM images of reversible Au NPs assemblies on pyrene-functionalized MWCNTs, taken before and after UV illumination.

of azobenzene-pyrene or azobenzene-naphthalene heterodimers: –8.7 and –6.1 kcal mol^{-1}; $\Delta E_{(E-Z)}$ = –2.2 and –3.1 kcal mol^{-1}, respectively. This emphasizes the importance of extended aromaticity, in particular, the presence of local electron deficiency in the flat, π–conjugated molecules—to assure the desired mutual coupling with (*Z*)-azobenzene electron pairs.

8. Conclusions

In summary, we demonstrated a light-controlled strategy for the reversible coassembly of binary low-dimensional nanostructures stabilized by aromatic ligands. By varying ligand aromaticity and photoactivity with tunable nanocarrier curvature and composition, we identified how π stacking, lone pair–π, and other weak interactions cooperate and compete to form supramolecular bonds that stabilize hybrid nanostructures. This insight enabled the light-driven formation of metastable magnetic assemblies with defined compositions and the controllable integration of nanoparticles with carbon nanotubes. The resulting coassembled nanostructures act as dynamic, magnetically addressable building blocks: they can serve as beads for magnetic separation, tunable catalyst supports, and adaptive platforms for molecular sensing, storage, and separation. More broadly, this work shows how orthogonal external stimuli: light and magnetic fields, can drive the assembly and disassembly of hybrid nanomaterials, opening pathways toward multifunctional architectures where reversibility, chemical selectivity, and physicochemical property modulation are essential for nanomaterial performance.

Supporting Information

Supporting Information is available from the Wiley Online Library or from the author.

Acknowledgements

M.M.W. acknowledges support from the National Science Centre, Poland under the OPUS grant number UMO-2019/35/B/ST5/04232. P.K. acknowledges support from the National Science Foundation (Division of Materials Research grant 1506886). The authors thank Dr. Magdalena Skompska and Dr. Rafal Jurczakowski for the use of their UV/Vis spectrophotometers, and Dr. Elzbieta Wyroba and her group for the use of their electron microscopes. The authors also thank Dr. Rafal Klajn for many insightful discussions and Dr. Aleksander Prominski and Dr. Robert Czochara for technical assistance.

© 2025 The Author(s). Advanced Functional Materials published by Wiley-VCH GmbH

16163028, 0, Downloaded from https://advanced.onlinelibrary.wiley.com/doi/10.1002/adfm.202504830 by Readcube (Labtiva Inc.), Wiley Online Library on [10/1/2025]. See the Terms and Conditions (https://onlinelibrary.wiley.com/terms-and-conditions) on Wiley Online Library for rules of use; OA articles are governed by the applicable Creative Commons License

Conflict of Interest

The authors declare no conflict of interest.

Author Contributions

M.S. conceived the idea, designed and performed the experiments, and characterized the samples. M.S., M.M.W., and P.K. discussed the results. M.S., Y.H., S.S., and P.K. carried out the computational modeling. B.S. prepared the samples for HAADF-STEM and EDS mapping. M.M.W. supervised the project. All authors discussed the results and contributed to manuscript writing.

Data Availability Statement

The data that support the findings of this study are available in the Supporting Information of this article.

Keywords

aromaticity, molecular photoswitches, nanomaterials, reversible self-assembly

Received: February 22, 2025
Revised: September 25, 2025
Published online:

[1] J. Jin, T. Iyoda, C. Cao, Y. Song, L. Jiang, T. J. Li, D. B. Zhu, *Angew. Chem., Int. Ed.* **2001**, *40*, 2135, https://doi.org/10.1002/1521-3773(20010601)40:11%3c2135::AID-ANIE2135%3e3.0.CO;2-O.
[2] J. E. Wittmann, L. M. S. Stiegler, C. Henkel, J. Träg, K. Götz, T. Unruh, D. Zahn, A. Hirsch, D. Guldi, M. Halik, *Adv. Mater. Interfaces* **2019**, *6*, 1801930, https://doi.org/10.1002/admi.201801930
[3] M. Li, C. Zhang, L. Fang, L. Shi, Z. Tang, H.-Y. Lu, C.-F. Chen, *ACS Appl. Mater. Interfaces* **2018**, *10*, 8225, https://doi.org/10.1021/acsami.8b00341.
[4] H. Zhao, S. Sen, T. Udayabhaskararao, M. Sawczyk, K. Kučanda, D. Manna, P. K. Kundu, J.-W. Lee, P. Král, R. Klajn, *Nat. Nanotechnol.* **2015**, *11*, 82, https://doi.org/10.1038/nnano.2015.256.
[5] X. Peng, J. Chen, J. A. Misewich, S. S. Wong, *Chem. Soc. Rev.* **2009**, *38*, 1076, https://doi.org/10.1039/b811424m.
[6] M. Ma, Y. Kuang, Y. Gao, Y. Zhang, P. Gao, B. Xu, *J. Am. Chem. Soc.* **2010**, *132*, 2719, https://doi.org/10.1021/ja9088764.
[7] Y. Tian, G. Zhu, *Chem. Rev.* **2020**, *120*, 8934, https://doi.org/10.1021/acs.chemrev.9b00687.
[8] J. Perego, J. Pedrini, C. X. Bezuidenhout, P. E. Sozzani, F. Meinardi, S. Bracco, A. Comotti, A. Monguzzi, *Adv. Mater.* **2019**, *31*, 1903309, https://doi.org/10.1002/adma.201903309.
[9] Q. Su, S. Pang, V. Alijani, C. Li, X. Feng, K. Müllen, *Adv. Mater.* **2009**, *21*, 3191, https://doi.org/10.1002/adma.200803808.
[10] K. Jayaramulu, S. Mukherjee, D. M. Morales, D. P. Dubal, A. K. Nanjundan, A. Schneemann, J. Masa, S. Kment, W. Schuhmann, M. Otyepka, R. Zbořil, R. A. Fischer, *Chem. Rev.* **2022**, *122*, 17241, https://doi.org/10.1021/acs.chemrev.2c00270.
[11] M. Nazarian-Samani, H.-K. Kim, S.-H. Park, H.-C. Youn, D. Mhamane, S.-W. Lee, M.-S. Kim, J.-H. Jeong, S. Haghighat-Shishavan, K.-C. Roh, S. F. Kashani-Bozorg, K.-B. Kim, *RSC Adv.* **2016**, *6*, 50941, https://doi.org/10.1039/C6RA07485E.
[12] X. Sun, C. Huang, L. Wang, L. Liang, Y. Cheng, W. Fei, Y. Li, *Adv. Mater.* **2020**, *33*, 2001105, https://doi.org/10.1002/adma.202001105.
[13] S. D. Priyadharshini, S. Manikandan, R. Kiruthiga, U. Rednam, P. S. Babu, R. Subbaiya, N. Karmegam, W. Kim, M. Govarthanan, *Environ. Pollut.* **2022**, *306*, 119377, https://doi.org/10.1016/j.envpol.2022.119377.
[14] S. R. Ahmed, J. Kim, T. Suzuki, J. Lee, E. Y. Park, *Biosens. Bioelectron.* **2016**, *85*, 503, https://doi.org/10.1016/j.bios.2016.05.050.
[15] S. Almohammed, S. T. Barwich, A. K. Mitchell, B. J. Rodriguez, J. H. Rice, *Nat. Commun.* **2019**, *10*, 2496, https://doi.org/10.1038/s41467-019-10393-9.
[16] J. Luo, H. D. Jang, J. Huang, *ACS Nano* **2013**, *7*, 1464, https://doi.org/10.1021/nn3052378.
[17] S.-H. Park, H.-K. Kim, S.-B. Yoon, C.-W. Lee, D. Ahn, S.-I. Lee, K. C. Roh, K.-B. Kim, *Chem. Mater.* **2014**, *27*, 457, https://doi.org/10.1021/cm5034244.
[18] G. G. Wildgoose, C. E. Banks, R. G. Compton, *Small* **2005**, *2*, 182, https://doi.org/10.1002/smll.200500324.
[19] J. Zou, Y. Lin, S. Wu, Y. Zhong, C. Yang, *Adv. Funct. Mater.* **2021**, *31*, 2100442, https://doi.org/10.1002/adfm.202100442.
[20] P. Serp, E. Castillejos, *ChemCatChem* **2009**, *2*, 41, https://doi.org/10.1002/cctc.200900283.
[21] S. Wittmann, A. Schätz, R. N. Grass, W. J. Stark, O. Reiser, *Angew. Chem., Int. Ed.* **2010**, *49*, 1867, https://doi.org/10.1002/anie.200906166.
[22] M. Grzelczak, L. M. Liz-Marzán, R. Klajn, *Chem. Soc. Rev.* **2019**, *48*, 1342, https://doi.org/10.1039/C8CS00787J.
[23] P. Král, H. Chan, L. Vukovic, S. Raj, S. Sen, Y. Han, M. Sawczyk, *Prog. Mater. Sci.* **2024**, *142*, 101225, https://doi.org/10.1016/j.pmatsci.2023.101225.
[24] R. Einholz, H. F. Bettinger, *Angew. Chem., Int. Ed.* **2013**, *52*, 9818, https://doi.org/10.1002/anie.201209722.
[25] L. Zhang, Y. Cao, N. S. Colella, Y. Liang, J.-L. Brédas, K. N. Houk, A. L. Briseno, *Acc. Chem. Res.* **2014**, *48*, 500, https://doi.org/10.1021/ar500278w.
[26] D. Wasserfallen, M. Kastler, W. Pisula, W. A. Hofer, Y. Fogel, Z. Wang, K. Müllen, *J. Am. Chem. Soc.* **2006**, *128*, 1334, https://doi.org/10.1021/ja056782j.
[27] B. Wang, Q. Zhu, D. Liao, C. Yu, *J. Mater. Chem.* **2011**, *21*, 4821, https://doi.org/10.1039/c0jm04527f.
[28] M. Quintana, M. Prato, *Chem. Commun.* **2009**, 6005, https://doi.org/10.1039/b915126e.
[29] W. A. Ogden, Z. Guan, *ChemSystemsChem* **2019**, *2*, 1900030.
[30] J. Leira-Iglesias, A. Sorrenti, A. Sato, P. A. Dunne, T. M. Hermans, *Chem. Commun.* **2016**, *52*, 9009, https://doi.org/10.1039/C6CC01192F.
[31] P. K. Kundu, D. Samanta, R. Leizrowice, B. Margulis, H. Zhao, M. Börner, T. Udayabhaskararao, D. Manna, R. Klajn, *Nat. Chem.* **2015**, *7*, 646, https://doi.org/10.1038/nchem.2303.
[32] D. Samanta, R. Klajn, *Adv. Opt. Mater.* **2016**, *9*, 1373, https://doi.org/10.1002/adom.201600364.
[33] R. E. Dawson, A. Hennig, D. P. Weimann, D. Emery, V. Ravikumar, J. Montenegro, T. Takeuchi, S. Gabutti, M. Mayor, J. Mareda, C. A. Schalley, S. Matile, *Nat. Chem.* **2010**, *2*, 533, https://doi.org/10.1038/nchem.657.
[34] T. J. Mooibroek, P. Gamez, J. Reedijk, *CrystEngComm* **2008**, *10*, 1501, https://doi.org/10.1039/b812026a.
[35] M. Egli, S. Sarkhel, *Acc. Chem. Res.* **2007**, *40*, 197, https://doi.org/10.1021/ar068174u.
[36] H. Kruse, K. Mrazikova, L. D'Ascenzo, J. Sponer, P. Auffinger, *Angew. Chem., Int. Ed.* **2020**, *59*, 16553, https://doi.org/10.1002/anie.202004201.
[37] C. He, M. Wang, B. Dong, Y. Su, X. H. Duan, L. Liu, *Green Synth. Catal.* **2024**, *5*, 117.
[38] G. A. DiLabio, E. R. Johnson, *J. Am. Chem. Soc.* **2007**, *129*, 6199, https://doi.org/10.1021/ja068090g.

© 2025 The Author(s). Advanced Functional Materials published by Wiley-VCH GmbH

16163028, 0, Downloaded from https://advanced.onlinelibrary.wiley.com/doi/10.1002/adfm.202504830 by Readcube (Labtiva Inc.), Wiley Online Library on [10/11/2025]. See the Terms and Conditions (https://onlinelibrary.wiley.com/terms-and-conditions) on Wiley Online Library for rules of use; OA articles are governed by the applicable Creative Commons License

[39] R. Klajn, P. J. Wesson, K. J. M. Bishop, B. A. Grzybowski, *Angew. Chem., Int. Ed.* **2009**, *48*, 7035, https://doi.org/10.1002/anie.200901119.
[40] J. Park, K. An, Y. Hwang, J.-G. Park, H.-J. Noh, J.-Y. Kim, J.-H. Park, N.-M. Hwang, T. Hyeon, *Nat. Mater.* **2004**, *3*, 891, https://doi.org/10.1038/nmat1251.
[41] E. Amstad, T. Gillich, I. Bilecka, M. Textor, E. Reimhult, *Nano Lett.* **2009**, *9*, 4042, https://doi.org/10.1021/nl902212q.
[42] H. Dieter Becker, *Chem. Rev.* **1993**, *93*, 145, https://doi.org/10.1021/cr00017a008.
[43] T. Zdobinsky, P. S. Maiti, R. Klajn, *J. Am. Chem. Soc.* **2013**, *136*, 2711, https://doi.org/10.1021/ja411573a.
[44] S. Das, P. Ranjan, P. S. Maiti, G. Singh, G. Leitus, R. Klajn, *Adv. Mater.* **2012**, *25*, 422, https://doi.org/10.1002/adma.201201734.
[45] S. Morup, M. F. Hansen, C. Frandsen, *Beilstein J. Nanotechnol.* **2010**, *1*, 182, https://doi.org/10.3762/bjnano.1.22.
[46] W. Wu, Q. He, C. Jiang, *Nanoscale Res. Lett.* **2008**, *3*, 397, https://doi.org/10.1007/s11671-008-9174-9.
[47] X. Fan, W. Zheng, D. J. Singh, *Light: Sci. Appl.* **2014**, *3*, 179, https://doi.org/10.1038/lsa.2014.60.
[48] M. Sawczyk, R. Klajn, *J. Am. Chem. Soc.* **2017**, *139*, 17973, https://doi.org/10.1021/jacs.7b09111.
[49] P. Crespo, R. Litrán, T. C. Rojas, M. Multigner, J. M. De La Fuente, J. C. Sánchez-López, M. A. García, A. Hernando, S. Penadés, A. Fernández, *Phys. Rev. Lett.* **2004**, *93*, 049903, https://doi.org/10.1103/PhysRevLett.93.087204.
[50] G. L. Nealon, B. Donnio, R. Greget, J.-P. Kappler, E. Terazzi, J.-L. Gallani, *Nanoscale* **2012**, *4*, 5244, https://doi.org/10.1039/c2nr30640a.
[51] X. Lu, Z. Chen, *Chem. Rev.* **2005**, *105*, 3643, https://doi.org/10.1021/cr030093d.
[52] H. Hinterwirth, S. Kappel, T. Waitz, T. Prohaska, W. Lindner, M. Lämmerhofer, *ACS Nano* **2013**, *7*, 1129, https://doi.org/10.1021/nn306024a.
[53] J. Ahrens, T. Bian, T. Vexler, R. Klajn, *ChemPhotoChem* **2017**, *1*, 230, https://doi.org/10.1002/cptc.201700009.
[54] S. Lee, K. Sim, S. Y. Moon, J. Choi, Y. Jeon, J.-M. Nam, S.-J. Park, *Adv. Mater.* **2021**, *33*, 2007668.
[55] M. Döbbelin, A. Ciesielski, S. Haar, S. Osella, M. Bruna, A. Minoia, L. Grisanti, T. Mosciatti, F. Richard, E. A. Prasetyanto, L. De Cola, V. Palermo, R. Mazzaro, V. Morandi, R. Lazzaroni, A. C. Ferrari, D. Beljonne, P. Samorì, *Nat. Commun.* **2016**, *7*, 11090, https://doi.org/10.1038/ncomms11090.
[56] O. Chovnik, R. Balgley, J. R. Goldman, R. Klajn, *J. Am. Chem. Soc.* **2012**, *134*, 19564, https://doi.org/10.1021/ja309633v.
[57] J. Schneider, J. X. Liu, V. E. Lee, R. K. Prudhomme, S. S. Datta, R. D. Priestley, *ACS Nano* **2022**, *16*, 16133, https://doi.org/10.1021/acsnano.2c04585.
[58] M. Bagiński, M. Tupikowska, G. González-Rubio, M. Wójcik, W. Lewandowski, *Adv. Mater.* **2019**, *32*, 1904581.
[59] A. M. Kalsin, M. Fialkowski, M. Paszewski, S. K. Smoukov, K. J. M. Bishop, B. A. Grzybowski, *Science* **2006**, *312*, 420, https://doi.org/10.1126/science.1125124.
[60] Y. Fan, J. Ma, Y. Li, X. Huang, S. Feng, D. Chen, *Chem. Mater.* **2024**, *36*, 4011, https://doi.org/10.1021/acs.chemmater.4c00134.
[61] A. H. Gröschel, A. Walther, T. Löbling, F. Schacher, H. Schmalz, A. H. E. Müller, *Nature* **2013**, *503*, 247, https://doi.org/10.1038/nature12610.
[62] V. Chandra, J. Park, Y. Chun, J. W. Lee, I.-C. Hwang, K. S. Kim, *ACS Nano* **2010**, *4*, 3979, https://doi.org/10.1021/nn1008897.
[63] E. Anaya-Plaza, A. Shaukat, I. Lehtonen, M. A. Kostiainen, *Adv. Healthcare Mater.* **2021**, *10*, 2001162, https://doi.org/10.1002/adhm.202001162.
[64] P. T. Yin, S. Shah, M. Chhowalla, K.-B. Lee, *Chem. Rev.* **2015**, *115*, 2483, https://doi.org/10.1021/cr500537t.
[65] E. V. Shevchenko, D. V. Talapin, N. A. Kotov, S. O'Brien, C. B. Murray, *Nature* **2006**, *439*, 55, https://doi.org/10.1038/nature04414.
[66] D. Eder, *Chem. Rev.* **2010**, *110*, 1348, https://doi.org/10.1021/cr800433k.
[67] S. Liu, L. Mei, X. Liang, L. Liao, G. Lv, S. Ma, S. Lu, A. Abdelkader, K. Xi, *ACS Appl. Mater. Interfaces* **2018**, *10*, 29467, https://doi.org/10.1021/acsami.8b08280.
[68] W. B. Rogers, W. M. Shih, V. N. Manoharan, *Nat. Rev. Mater.* **2016**, *1*, 16008, https://doi.org/10.1038/natrevmats.2016.8.

© 2025 The Author(s). Advanced Functional Materials published by Wiley-VCH GmbH

16163028, 0, Downloaded from https://advanced.onlinelibrary.wiley.com/doi/10.1002/adfm.202504830 by Readcube (Labtiva Inc.), Wiley Online Library on [10/11/2025]. See the Terms and Conditions (https://onlinelibrary.wiley.com/terms-and-conditions) on Wiley Online Library for rules of use; OA articles are governed by the applicable Creative Commons License